ORIGINAL ARTICLE

Identification of the failure modes of CFRP shear-strengthened reinforced concrete beams by the finite element method

Identificação dos modos de ruptura de vigas de concreto armado reforçadas ao cisalhamento com PRFC pelo método dos elementos finitos

Palloma Borges Soares[a] ID
Paula Manica Lazzari[a] ID
Américo Campos Filho[a] ID
Bruna Manica Lazzari[b] ID
Alexandre Rodrigues Pacheco[a] ID

[a]Universidade Federal do Rio Grande do Sul, Programa de Pós-Graduação em Engenharia Civil, Porto Alegre, RS, Brasil
[b]Pontifícia Universidade Católica do Rio Grande do Sul, Escola Politécnica, Porto Alegre, RS, Brasil

Abstract: The rehabilitation and strengthening of concrete structures using carbon fiber reinforced polymers (CFRP) has become an interesting alternative for a series of important aspects. This material has a low specific weight, high tensile strength, corrosion and fatigue resistance, a high modulus of elasticity, and is a versatile material, with ease and speed in its application. Nevertheless, its consideration and design tend to require more sophisticated analyses to evaluate and predict the behavior of the strengthened structural element. For this reason, numerical methods, such as the Finite Element Method (FEM), can be used in such complex analyses to simulate to a high degree the actual performance of the structure. Thus, this work presents computer simulations of reinforced concrete beams shear strengthened with CFRP through the Finite Element Method in a customized ANSYS model. Special attention is given to the bond behavior between the CFRP sheets and the concrete surface of the beams through contact elements and bilinear cohesive zone models, which allowed for the identification of the debonding failure modes. Twenty-one reinforced concrete beams reported in the literature were simulated: twelve simply supported and nine continuous, with and without CFRP shear strengthening. The beams showed failure modes in shear, bending, concrete splitting, and debonding of the strengthening CFRP sheets. The numerical model developed predicted with good accuracy the beams' behavior in terms of load vs. displacement, load vs. strain, as well as their ultimate loads and failure modes.

Keywords: strengthened reinforced concrete beams, carbon fiber reinforced polymers, finite element method, ANSYS, failures modes.

Resumo: A crescente necessidade de reabilitar e reforçar estruturas de concreto armado, assim como os problemas apresentados por técnicas de reforço tradicionais, tornou a utilização de polímeros reforçados com fibras de carbono (PRFC) uma alternativa interessante, uma vez que este material apresenta propriedades como baixo peso específico, elevada resistência à tração, à corrosão e à fadiga, alto módulo de elasticidade, assim como versatilidade, facilidade e rapidez de execução. A fim de avaliar e prever o comportamento do PRFC, é necessário realizar uma análise mais aprofundada dos elementos estruturais reforçados com esse material. Para isso, utilizam-se métodos numéricos, como é o caso do método de elementos finitos (MEF), que permite analisar estruturas complexas, bem como realizar análises não lineares de estruturas de concreto armado. Diante disso, o objetivo deste trabalho é apresentar uma modelagem computacional de vigas de concreto armado, reforçadas ao cisalhamento com PRFC, através do método dos elementos finitos com o emprego do software ANSYS customizado. Especial atenção foi dada ao comportamento da aderência entre o reforço e a viga de concreto, através da utilização de elementos de contato e de modelos de zona coesiva bilineares, possibilitando identificar, durante as simulações computacionais, falhas por perda de aderência do sistema de reforço.

P. B. Soares, P. M. Lazzari, A. Campos Filho, B. M. Lazzari, and A. R. Pacheco

Neste estudo foram testadas vinte e uma vigas de concreto armado reportadas na literatura, doze biapoiadas e nove contínuas, com e sem reforço ao esforço cortante com PRFC. Estas vigas apresentaram modos de ruptura por cisalhamento, por flexão, por fendilhamento do concreto, assim como pelo descolamento da camada de reforço. Constatou-se que os modelos numéricos desenvolvidos foram capazes de prever com boa precisão o comportamento das vigas simuladas, tanto em termos de carga-deslocamento e carga-deformação, como a carga e o modo de ruptura.

Palavras-chave: reforço estrutural de vigas de concreto armado, polímeros reforçados com fibras de carbono, método dos elementos finitos, ANSYS, modos de ruptura.

1 INTRODUCTION

A reduction in the performance of concrete structures tends to occur along their lifespan because of many factors and, eventually, they may present deficient strength to resist their design forces. Several strengthening methods can be applied to structural elements, such as externally bonded steel plates or fiber-based composite materials. The latter consists of the application of composite materials known as Fiber Reinforced Polymer (FRP), which present properties of low density, high tensile strength, corrosion resistance, high fatigue resistance, and high-impact resistance. Among the types of composite materials, carbon fiber reinforced polymers (CFRP) are the most used for structural strengthening since carbon fibers offer the best mechanical properties. Therefore, according to Dias [1] and Mhanna et al. [2], significant increases in the load capacity of structural elements are obtained through a small amount of strengthening.

The finite element method (FEM) can evaluate de actual behavior of structural elements strengthened with CFRP. Using FEM, it is possible to simulate various geometric arrangements, boundary and loading conditions, and analyze the bond between concrete and the strengthening system.

This work aims to demonstrate the viability of computational simulations of the behavior of reinforced concrete beams shear-strengthened with CFRP via the Finite Element Method through the software ANSYS, version 19.2. As recommended by Soares [3], special attention is given to the identification of the different failure modes of the simulated beams.

2 MATERIAL CONSTITUTIVE MODELS

Concrete constitutive models implemented by Lazzari et al. [4], Lazzari et al. [5], and Hoffman et al. [6], were adopted in the ANSYS UPF (User Programmable Features) customization tool. An elastoplastic model with hardening represented the concrete behavior under compression, while a linear elastic model up to crack formation described the concrete behavior under tension, with a smeared crack model considered afterward.

The concrete under compression model comprises a failure criterion, a plastification criterion, and a hardening rule. The failure surface of Ottosen [7] was adopted for the failure criterion, as recommended by the *fib* Model Code 2010 [8]. Additionally, the concrete under compression was considered to present an isotropic hardening, and the plastification surface had the same shape as the rupture surface.

The movement of the plastification surfaces (loading surfaces) during the plastic deformation was given by the hardening rule. This rule was determined by the relation between the effective stress and the effective plastic strain, allowing extrapolations of simple uniaxial tests to multiaxial situations. The curve corresponding to the stress vs. strain diagram for the concrete under uniaxial compression proposed by the *fib* Model Code 2010 [8] was adopted as a hardening rule for those extrapolations.

The model suggested by Hinton [9] was used to represent the behavior of the concrete under tension, with the concrete modeled as an elastic material with softening, i.e., behaving elastically until rupture, when a smeared cracking model with tension stiffening takes place. The smeared cracking model was specified by a cracking criterion, a rule for the concrete contribution between cracks, and a model for transferring shear stresses.

Each local direction's stiffness was considered independently when a determined integration point cracked. Therefore, stress vs. strain diagrams corresponding to uniaxial internal forces were used for each of the two principal directions in the crack plane. The stress vs. strain diagram for concrete under compression was adopted when a shortening occurred in one of those directions, and the diagram for concrete under tension when an elongation was detected.

Titello [10] introduced a new criterion to the cracked concrete model where the consideration of the tension stiffening would depend on the reinforcement orientation. This would provide a better result when analyzing beams without shear reinforcement, which happens in some cases studied herein. Thus, when no stirrups were used, the effect was considered only for the vertical cracks, i.e., the ones with an inclination up to 15° with the vertical direction.

P. B. Soares, P. M. Lazzari, A. Campos Filho, B. M. Lazzari, and A. R. Pacheco

Typically, steel rebars are considered to resist only axial forces in reinforced concrete structures. Therefore, a uniaxial model was adopted to describe the behavior of the steel reinforcements. According to Lazzari et al. [11], and Machado et al. [12], rebar products differ due to their fabrication process: there are laminated products with well-defined yielding plateaus, which are modeled with a perfect elastoplastic model; and cold-formed steel products, which are modeled with an elastoplastic model with linear hardening up from 0.85 of its yielding stress.

Several approaches can be considered to numerically model interfaces, with the Cohesive Zone Model (CZM) as the typical choice when the thickness of the bonding region is negligible. This model is commonly used in analyses of problems that involve composite materials since it avoids singularities and can be easily implemented numerically in Finite Element formulations. Additionally, CZM uses relative stress-slip relation for interface analyses [13], [14].

Medeiros [15] mentions that most numerical simulations consider that the interface between concrete and CFRP is dominated by tangential slips, i.e., Mode II of separation [16]. Therefore, a Mode II behavior is considered in this work, with bilinear tangential stress vs. slip relation, as illustrated in Figure 1.
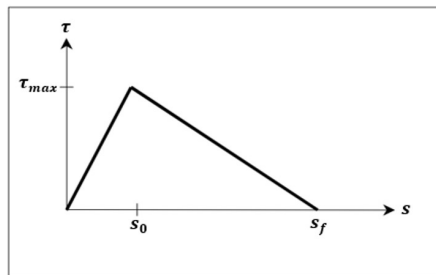

Figure 1. Bilinear relation between bonding stress and slip [17].

The bilinear model by Lu et al. [18] was considered to evaluate the parameters of the formulation implemented in ANSYS. This model can be considered to represent the concrete-strengthening interface behavior. To accomplish that, the curve that governs the behavior is determined as a function of the bond stress and its corresponding slip. Therefore, the Equations 1-10 mathematically describe the bilinear model considered in this work:

$$\tau = \tau_{max} \frac{s}{s_0}, s \leq s_0 \tag{1}$$

$$\tau = \tau_{max} \frac{s_f - s}{s_f - s_0}, s_0 < s \leq s_f \tag{2}$$

$$\tau = 0, s > s_f \tag{3}$$

$$s_f = \frac{2 G_f}{\tau_{max}} \tag{4}$$

$$\tau_{max} = 1{,}5\beta_w f_t \tag{5}$$

$$\beta_w = \sqrt{\frac{2{,}25 - b_f/b_c}{1{,}25 + b_f/b_c}} \tag{6}$$

$$f_t = 0{,}395 f_{cu}^{0,55} \tag{7}$$

$$f_{cu} = \frac{f_c}{0{,}76} \tag{8}$$

$$s_0 = 0{,}0195\beta_w f_t \tag{9}$$

$$G_f = 0{,}308\beta_w^2 \sqrt{f_t} \tag{10}$$

The coefficient β_w is the factor that correlates the CFRP strengthening width (b_f) and the concrete beam width (b_c); f_t is the concrete tensile strength related to the concrete cube compressive strength (f_{cu}). Equation 8 correlates strength f_{cu} with the mean compressive strength (f_c). The measured slip when the bonding stress is at a maximum (s_0) is defined in Equation 9. Lastly, the measured slip when displacement occurs (s_f) is calculated from the fracture energy in the interface (G_f) and from the maximum bonding stress (τ_{max}), as shown in Equation 4.

3 COMPUTATIONAL MODEL

The Finite Element Method was used to carry out the numerical simulation since it is one of the most efficient ways to analyze the non-linear behavior of concrete and steel materials. The method also considers failures due to bonding loss of strengthening systems by introducing particular finite elements in the interface regions. ANSYS version 19.2 was used to carry out these finite element analyses. It presents a library with many finite elements that can be chosen according to the type of problem to be analyzed.

The 3D quadratic finite element SOLID186 was considered to represent the concrete. This element has 20 nodes with three degrees of freedom each, corresponding to the translations in the X, Y, and Z axes. This finite element was chosen because of its good answer under coarser meshes, which considerably reduces the processing time during structural analyses. Additionally, the element presents compatibility with the finite element REINF264, which is needed to represent reinforced concrete with its discretized rebars. REINF264 is a reinforcing finite element that can be used together with beam elements, shells, and even solid elements. This element is adequate for simulations of reinforcing fibers randomly oriented, with every fiber modeled individually and presenting only axial stiffness. The nodal coordinates, degrees of freedom, and connectivities of element REINF264 are identical to those of the base finite element. In this work, the element REINF264 is used to discretize the steel rebars embedded in concrete in a perfectly bonded incorporated approach.

The finite element SHELL281 was used to model the strengthening CFRP sheets. This finite element presents 8 nodes with 6 degrees of freedom each, considering membrane and bending stiffnesses. However, only the membrane stiffnesses were defined for the element since the CFRP sheets would develop mainly tension forces, resulting in only three degrees of freedom per node (translations in the X, Y, and Z axes).

An association of a contact element and a target element was adopted to model the interface between concrete and the strengthening system. Thus, the finite elements CONTA174 and TARGE170 were used to represent the slip that may occur in the interface between the solid and the shell elements.

Regarding the constitutive models, an elastoplastic model with cracking was implemented for the concrete in the USERMAT3D subroutine, which is available for customization purposes in the software through FORTRAN commands. This subroutine is compatible with the 3D element used to represent the concrete, i.e., SOLID186. The constitutive model BISO (*Bilinear Isotropic Hardening*), was used to represent the reinforcing bars and was already available in the ANSYS library.

4 STRUCTURAL CHARACTERISTICS

Khalifa [19] tested twenty-one full-scale reinforced concrete beams with a rectangular section and designed to collapse under shear. The beams were grouped into two main series called A and B. Series A comprised twelve beams simply supported, and series B by nine continuous beams. The A-series beams were subdivided into two main groups (A-SW and A-SO) depending on the existence or not of stirrups in the right half of the beam. The A-SW group consisted of four beams, which had steel stirrups along the entire length of the beam, and the dimensions and details of this group are shown in Figure 2a. The A-SO group was composed of eight beams, which did not have stirrups in the right half of the beam, as shown in Figure 2b. As shown in Figure 2c, all beams had the same cross-section of 150 x 305 mm, and upper, and bottom reinforcement was composed of two 32mm in diameter rebars. The shear reinforcement was formed of 10mm in diameter stirrups spaced by 80mm and 125mm, as shown in Figure 2a-2b.
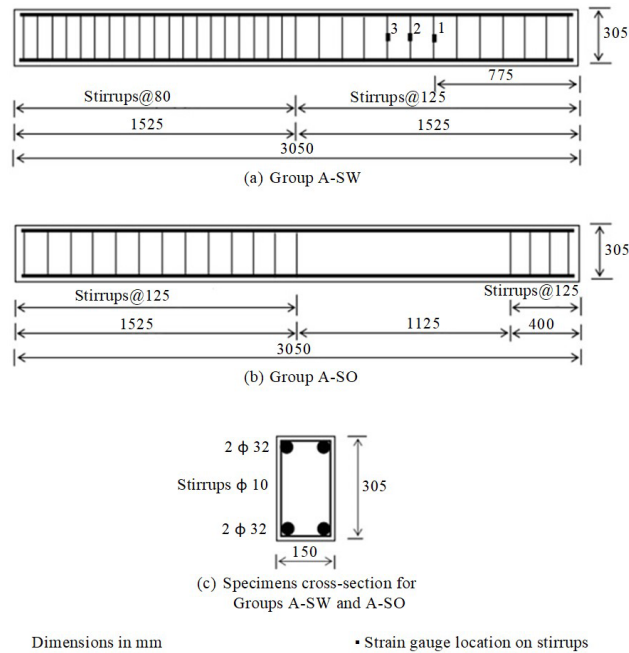
Figure 2. Configuration and reinforcement details for Series A beams [20].

Series B was divided into three groups: B-CW, B-CO, and B-CF. Each group had different rates for flexural and shear reinforcement. The B-CW group is composed of two beams with stirrups along the entire length of the beam. Part of the right span had less shear reinforcement to force shear failure in this position. The dimensions and details of this group are shown in Figure 3a. The B-CO group consists of three beams with longitudinal reinforcement equal to group B-CW. These beams had no stirrups in the shear span tested, as shown in Figure 3b. The four beams of the B-CF group had no shear reinforcement, as can be seen in Figure 3c. Table 1 presents the properties of the materials of the beams in series A and B.
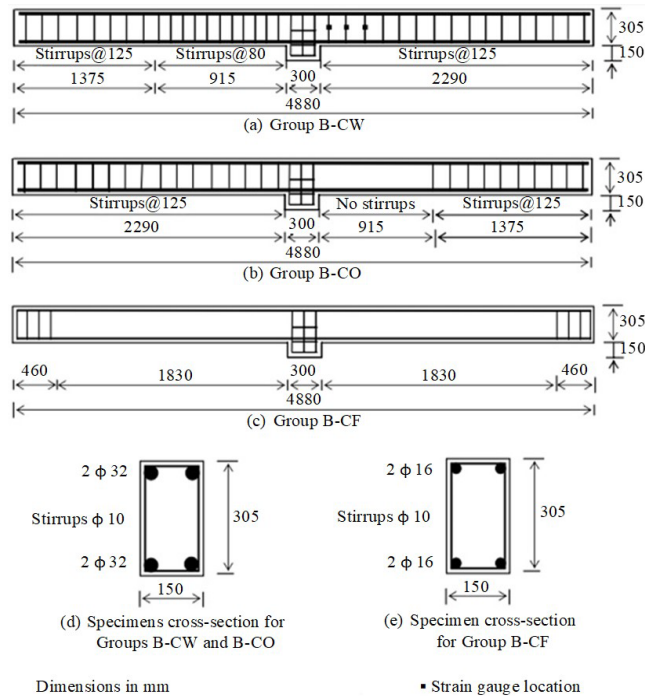
Figure 3. Configuration and reinforcement details for Series B beams [21].

Table 1. Material properties [21].

Material	Specification	Compressive strength (MPa)	Yielding stress (MPa)	Ultimate tensile strength (MPa)	Modulus of elasticity (GPa)
Concrete	Group A-SW	19.3	-	2.2	20
	Group A-SO	27.5	-	2.7	25
	Group B-CW	27.5	-	2.7	25
	Group B-CO	20.5	-	2.2	22
	Group B-CF	50.0	-	4.1	33
Steel	$\varphi = 32$ mm	-	460	730	200
	$\varphi = 16$ mm	-	430	700	200
	$\varphi = 10$ mm	-	350	530	200
CFRP	$t_{fa} = 0.165$ mm	-	-	3790	228
	$t_{fb} = 0.165$ mm	-	-	3500	228

Both series SW and SO were subdivided according to their shear span to effective depth ratio (a/d), and since a/d ratios of 3 and 4 were considered, four subgroups were then obtained: SW3, SW4, SO3, and SO4. Four of the twelve tested beams were not strengthened with CFRP sheets, i.e., one in each of the subgroups, denominated SW3-1, SW4-1, SO3-1, and SO4-1. The eight beams that were strengthened with externally bonded CFRP laminates in three different configurations (see Figure 4) were denominated SW3-2, SW4-2, SO3-2, SO3-3, SO3-4, SO3-5, SO4-2, and SO4-3.
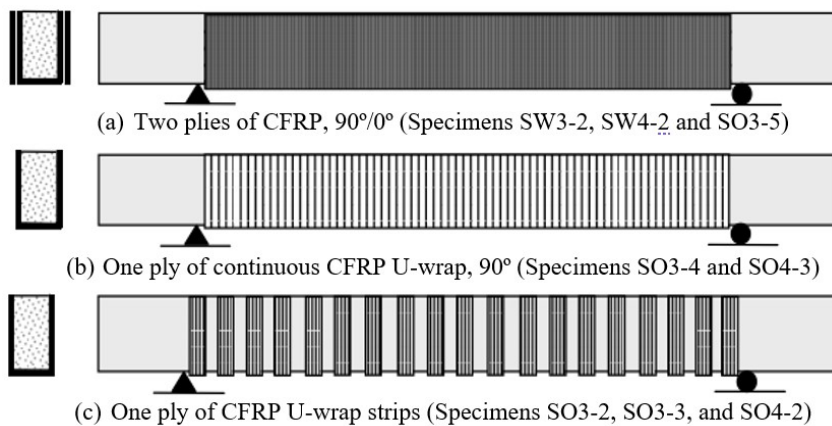

(a) Two plies of CFRP, 90º/0º (Specimens SW3-2, SW4-2 and SO3-5)

(b) One ply of continuous CFRP U-wrap, 90º (Specimens SO3-4 and SO4-3)

(c) One ply of CFRP U-wrap strips (Specimens SO3-2, SO3-3, and SO4-2)

Figure 4. Schematic representation of CFRP strengthening schemes for beam specimens of Series A [20].

All Series A beams were four-point bending tested by applying a load to a steel load-distribution element to produce two concentrated loads at certain positions. These positions are represented in Figure. 5a for the beams with an a/d ratio equal to 3 and, in Figure 5b, for the beams with an a/d ratio equal to 4. Four LVDTs (*linear variable differential transformers*) were used to measure the vertical displacements at specific points of the beams, as shown in Figure 5. Two of them were positioned at midspan on each side of the beams, while the other two were positioned at the supports.
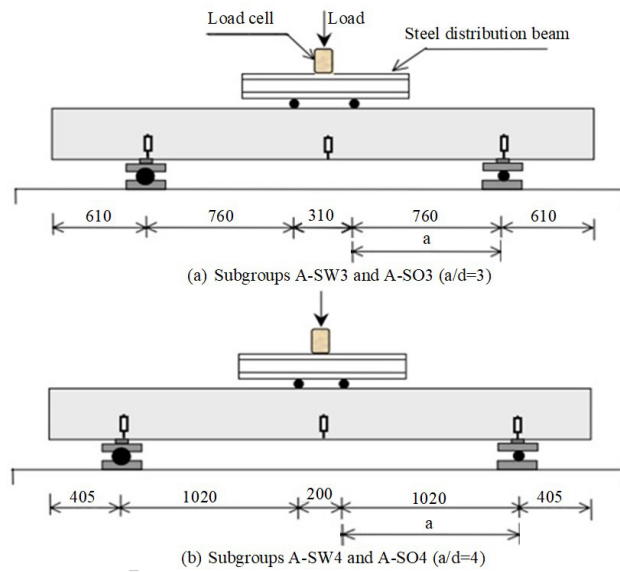
P. B. Soares, P. M. Lazzari, A. Campos Filho, B. M. Lazzari, and A. R. Pacheco

Figure 5. Schematic representation of test set-up for Series A [20].

For group B, one beam from each subgroup was not strengthened with CFRP. These beams were called B-CW1, B-CO1, and B-CF1, as shown in Figure 6a. The other six beams were strengthened with CFRP, following four different configurations, as shown in Figure 6, and were called B-CW2, B-CO2, B-CO3, B-CF2, B-CF3, and B-CF4. All beams in Series B were tested as continuous and subjected to concentrated loads in the center of each span, as can be seen in Figure 6. Five LVDTs were used in each beam: two fixed at midspan and the other three at the supports.
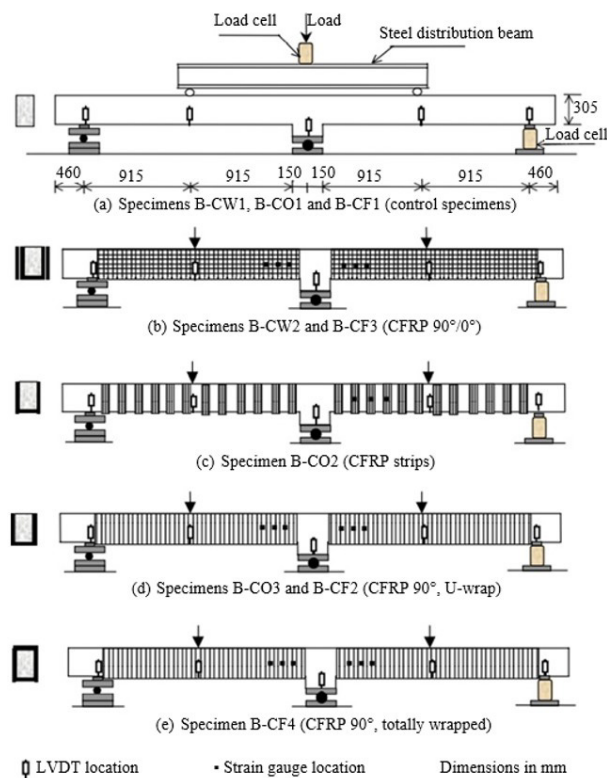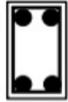
Figure 6. Strengthening schemes and test set-up for Series B beams [21].

Table 2 summarizes the characteristics of the beams in Series A and B, such as dimensions and details of the cross-sections, shear span and effective depth ratio (a/d), concrete compressive strength, shear reinforcement, and CFRP strengthening configurations.

Table 2. Summary of beam characteristics [21].

Nº	Specimen designation	Structural system and cross-section details	a/d ratio	Concrete strength (MPa)	Shear reinforcement	
					Steel stirrups in the test region	CFRP
1	A-SW3-1	Simply supported beams 2 φ 32 2 φ 32	3	19.3	φ 10@125mm	-
2	A-SW3-2		3	19.3	φ 10@125mm	Two plies (90°/0°)
3	A-SW4-1		4	19.3	φ 10@125mm	-
4	A-SW4-2		4	19.3	φ 10@125mm	Two plies (90°/0°)
5	A-SO3-1		3	27.5	-	-
6	A-SO3-2		3	27.5	-	U-wrap strips, 50 @ 125mm
7	A-SO3-3		3	27.5	-	U-wrap strips, 75 @ 125mm
8	A-SO3-4		3	27.5	-	One-ply continuous U-wrap
9	A-SO3-5		3	27.5	-	Two plies (90°/0°)
10	A-SO4-1		4	27.5	-	-
11	A-SO4-2		4	27.5	-	U-wrap strips, 50 @ 125mm
12	A-SO4-3		4	27.5	-	One-ply continuous U-wrap
13	B-CW1	Continuous beams 2 φ 32 2 φ 32	3.6	27.5	φ 10@125mm	-
14	B-CW2		3.6	27.5	φ 10@125mm	Two plies (90°/0°)
15	B-CO1		3.6	20.5	-	-
16	B-CO2		3.6	20.5	-	U-wrap strips, 50 @ 125mm
17	B-CO3		3.6	20.5	-	One-ply continuous U-wrap
18	B-CF1	Continuous beams 2 φ 16 2 φ 16	3.6	50	-	-
19	B-CF2		3.6	50	-	One-ply continuous U-wrap
20	B-CF3		3.6	50	-	Two plies (90°/0°)
21	B-CF4		3.6	50	-	One-ply totally wrapped

5 NUMERICAL MODEL

In the computational analysis of the beams tested by Khalifa [19], only half of the width of the beams was modeled since they present symmetry of geometry and load along the cross-section. Hexahedrical 20-node quadratic finite elements (SOLID186) were used to represent concrete. REINF264 elements discretized inside the solid elements represented the embedded reinforcement in the beams. Furthermore, at the loading points and supports, plates of SOLID186 elements, with dimensions of 10 x 2 x 7.5 cm, were included to avoid the concentration of stresses at those locations.

Figure 7 presents the mesh discretization for simply supported beams. Figure 7a shows the beam without CFRP strengthening and with an a/d ratio equal to 4 (A-SO4-1), and Figure 7b shows the A-SW3-2 beam, which is strengthened with continuous CFRP and had an a/d ratio equal to 3. Figure 8 illustrates the characteristics of continuous beams with strengthening in bands and with total involvement. Figure 8a corresponds to the model of the B-CO2 beam, and Figure 8b shows the B-CF4 beam. Figure 9a-9b present the cross-sections of the beams without strengthening. Figure 9c-9d show the cross-sections of the beams strengthened in a U-shape and with total wrapping, respectively.
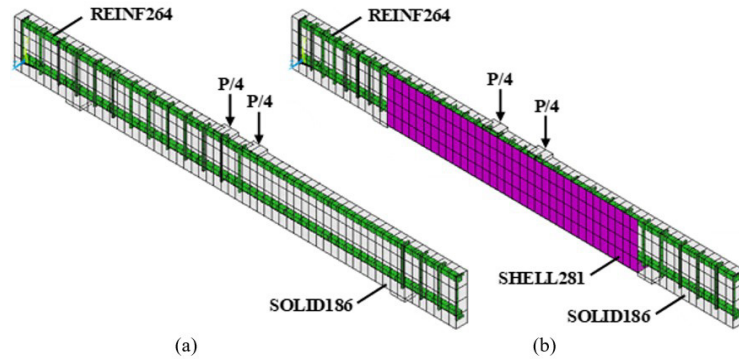
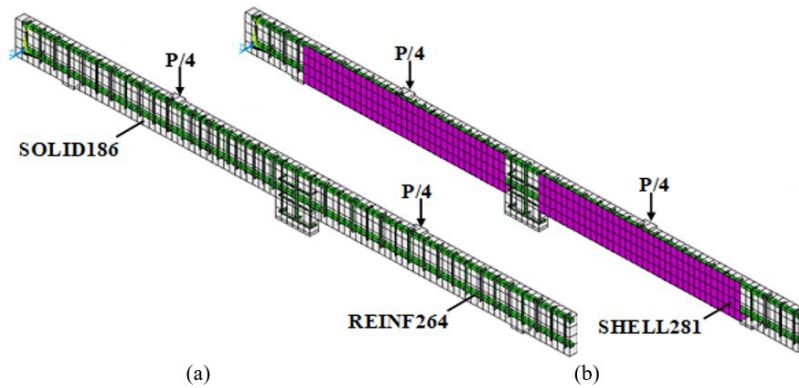**Figure 7.** Finite element discretization of the beams: (a) A-SO4-1, and (b) A-SW3-1.

Figure 8. Finite element discretization of the beams: (a) B-CO2, and (b) B-CF4.
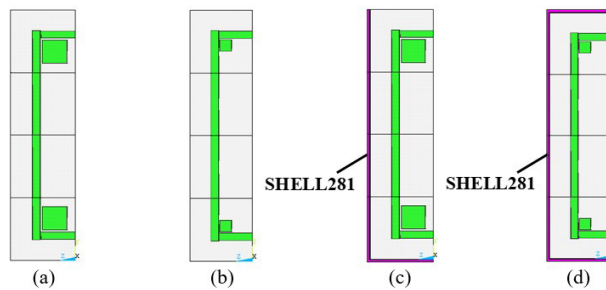

Figure 9. Cross-sections of the beams: (a) A-SW, A-SO, B-CW, and B-CO without CFRP; (b) B-CF without CFRP; (c) CFRP U-wrap; and (d) CFRP, totally wrapped.

The adhesive, used to bond the CFRP composite to the concrete surface, was modeled in two layers of 20-node quadratic hexahedral finite elements (SOLID186). One layer was modeled on the surface of the SOLID186 elements (concrete) and the other on the surface of the SHELL281 elements (CFRP composite), enabling the positioning of CONTA174 and TARGE170 elements in these adhesive layers, as can be seen in Figure 10.
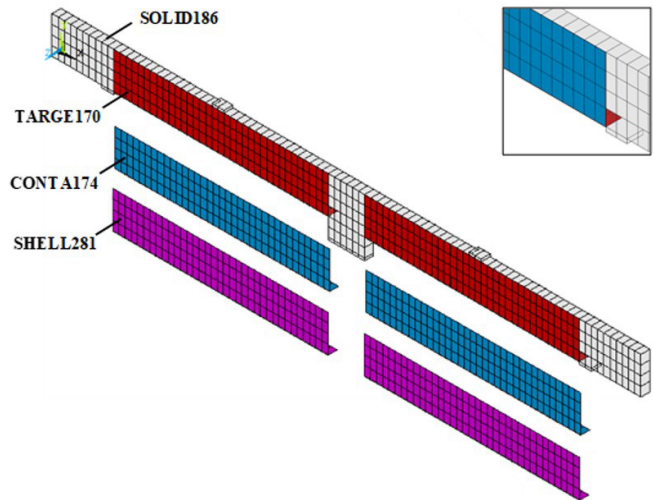
Figure 10. CONTA174 and TARGE170 elements for modeling beam B-CW2.

The interface properties were determined from the model and formulation proposed by Lu et al. [18]. Substituting the parameters of the beams tested by Khalifa [19] in the formulation presented in item 2, it was possible to determine the values of maximum bond stress, tangential interface stiffness, and maximum slip for each group of beams, as shown in Table 3.

Table 3. Interface model parameters.

Group	Maximum bonding stress τ_{f1} (kN/cm²)	Tangential stiffness K_t (kN/cm³)	Maximum slip s_0 (cm)
A-SW	0.317	77	0.0182
A-SO	0.366	77	0.0169
B-CW	0.366	77	0.0169
B-CO	0.324	77	0.0180
B-CF	0.479	77	0.0148

6 RESULT ANALYSIS

This item presents a comparative analysis between the numerical and the experimental results of Khalifa [19], Khalifa and Nanni [20], Khalifa et al. [21], and Khalifa et al. [22] for beams in Series A and B. Load vs. displacement diagrams in the central section of each beam are presented, as well as stresses and strains in concrete, reinforcement, and CFRP strengthening. In addition, the behavior of the interface is analyzed through the results of bond stresses and slips obtained from the contact elements.

The short-term behavior for all simulated beams was determined. It is essential to point out that the values presented in this item are net values, i.e., the values corresponding to self-weight have been discounted. Next, the results of only some beams analyzed according to the type of failure observed are presented. Complete results can be found in Soares [3].

6.1 Shear failure

Figure 11 presents the load vs. displacement diagram for the experimental tests and the numerical analyses of the simply supported beams A-SW3-1, A-SO4-1, and the continuous beam B-CF1.
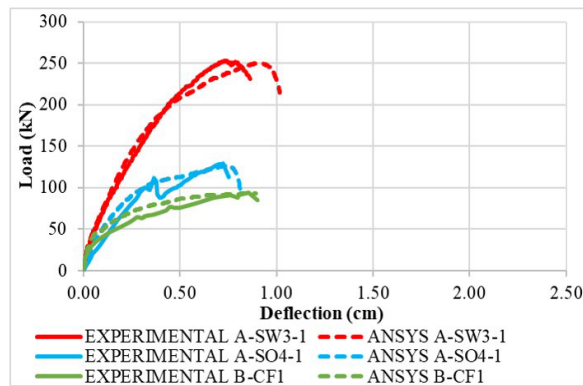
Rev. IBRACON Estrut. Mater., vol. 16, no. 3, e16304, 2023

10/21

Figure 11. Load vs. displacement diagram of beams with shear failure.

Regarding the failure mode, it was found, through the simulations, that these beams had a shear failure. It was observed through the stress distribution in the reinforcements, Figure 12-12b (stirrups of the shear span of interest) for beam A-SW3-1, that the stirrups reached the yield stress (35 kN/cm^2) before yielding in the longitudinal reinforcement (46 kN/cm^2), indicating shear failure. As for beam A-SO4-1, it was possible to observe that the concrete reached a high principal tensile deformation at the web, Figure 13, which indicated shear failure due to the formation of a diagonal crack. This failure was predictable since the analyzed beam did not have shear reinforcement in the shear span. Similar behavior was observed in the failure of beam B-CF1, with high elongations in its web, Figure 14, indicating failure by shear. These results followed what was observed in the experimental tests carried out by Khalifa [19]. Figure 15 illustrates the failure of beams A-SW3-1 and B- CF1.

(a) P = 250 kN

(b) P = 250 kN
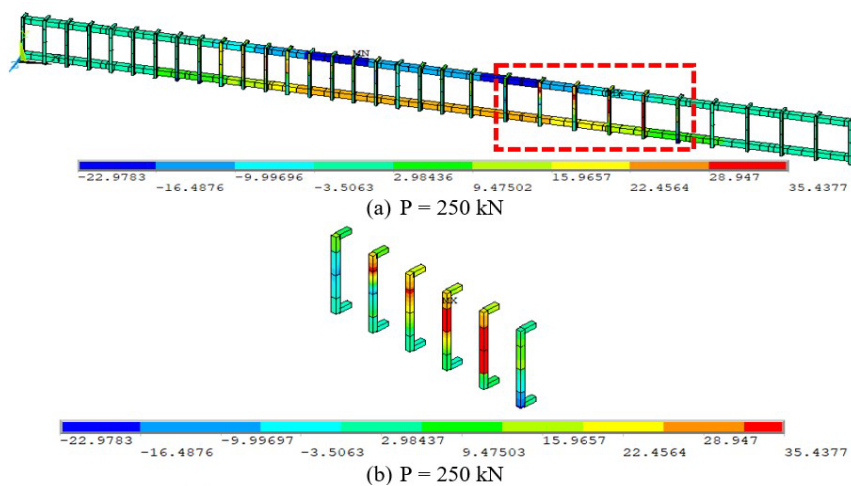
Figure 12. Stress σ_x in the reinforcement of beam A-SW3-1 (kN/cm^2).

(a) Side face

(b) Cross-section symmetry plane
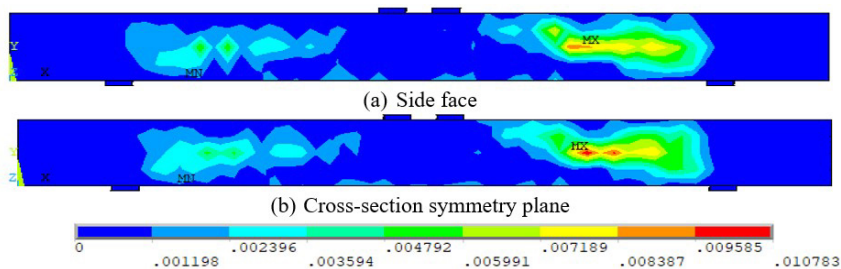
Figure 13. Principal strain ε_1 in the concrete of beam A-SO4-1 (cm/cm).
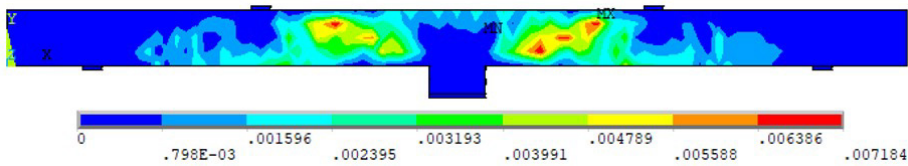
Figure 14. Principal strain ε_1 in the concrete of beam B-CF1 (cm/cm).

| (a) A-SW3-1 | (b) B-CF1 |

Figure 15. Failure modes observed in the beam tests [19].

6.2 Failure by splitting

Figure 16 presents the load vs. midspan deflection diagram, for the experimental tests and the numerical analyses, of beams A-SW3-2, A-SW4-2, and B-CW2.
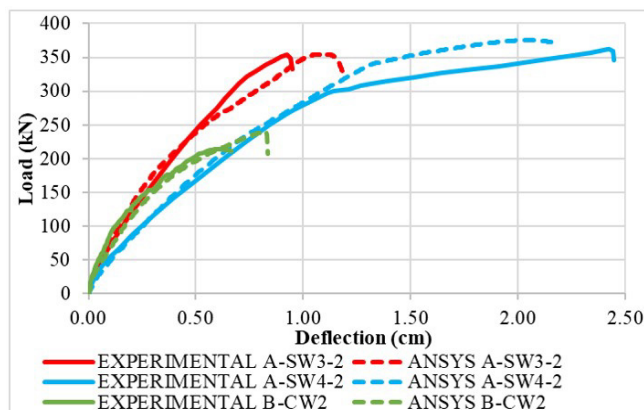

Figure 16. Load vs. midspan deflection diagram for the beams with splitting failure.

Results from the computational analysis, Figure 17, show that the stress in the concrete in the Z-direction (beam width) for beam A-SW3-2 reaches very high values at failure, characterizing failure by concrete splitting. A similar situation occurred for beams A-SW4-2 and B-CW2, where it was verified that the concrete presented, in the plane of symmetry, principal tensile strains with very high values, as shown in Figure 18 and Figure 19, respectively. This corroborates with what was determined in the experimental tests, where the failure occurred due to concrete splitting, as seen in Figure 20a for beam A-SW3-2 and Figure 20b for beam B-CW2.
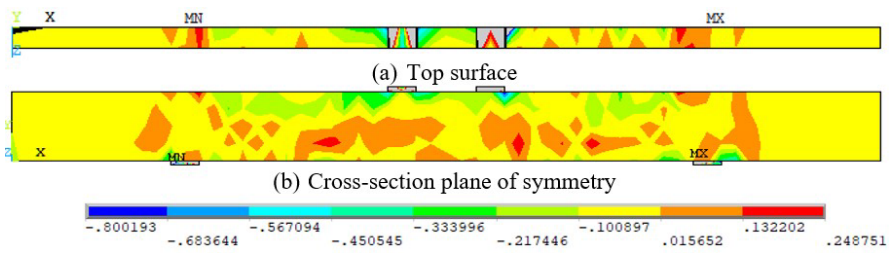
(a) Top surface

(b) Cross-section plane of symmetry

Figure 17. Stress σ_z in concrete for beam A-SW3-2 (kN/cm^2).

(a) Lateral face

(b) Cross-section plane of symmetry
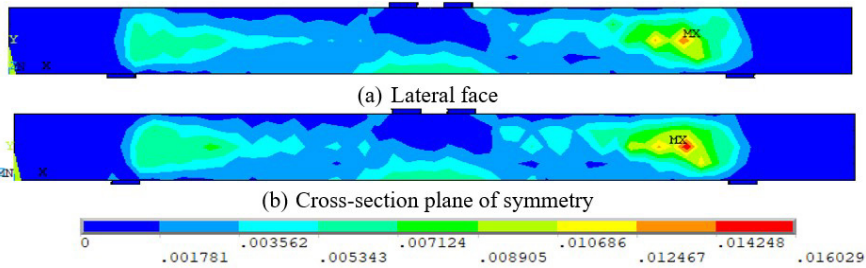
Figure 18. Principal strain ε_1 in concrete for beam A-SW4-2 (cm/cm).

(a) Lateral face

(b) Cross-section plane of symmetry
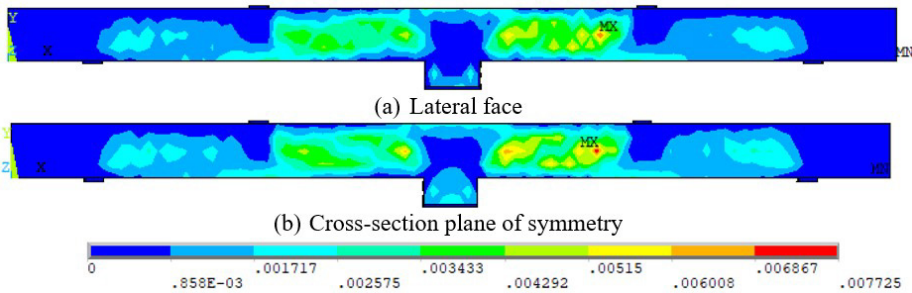
Figure 19. Principal strain ε_1 in concrete for beam B-CW2 (cm/cm).
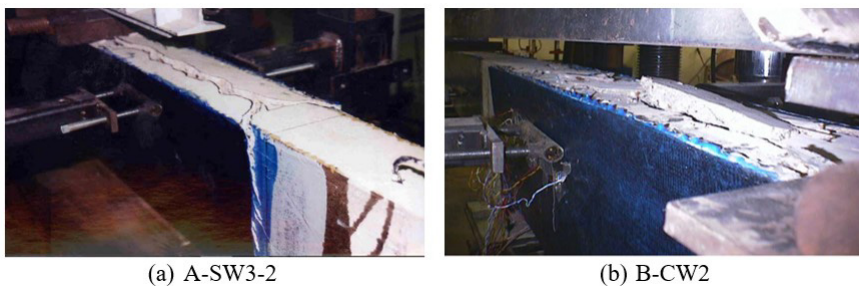
(a) A-SW3-2   (b) B-CW2
Figure 20. Failure modes observed in the experiments [19].

6.3 Failure by CFRP debonding

The diagram load vs. midspan deflection in Figure 21 compares numerical and experimental results for beams A-SO3-3, ASO4-2, and B-CO2. Figure 22 shows the stress distribution in the lateral strengthening of beam A-SO3-3, where it is possible to observe that the highest stress value in the shear span occurs for a load of 188 kN, Figure 22a. As the load increases, this tensile stress decreases, indicating failure in the connection between the strengthening and the beam surface. At this time, a reduction in the stiffness of the load-displacement curve is observed. Then, an increase in stresses in the strengthening on the opposite side of the beam occurs when the ultimate load is reached, Figure 22b.
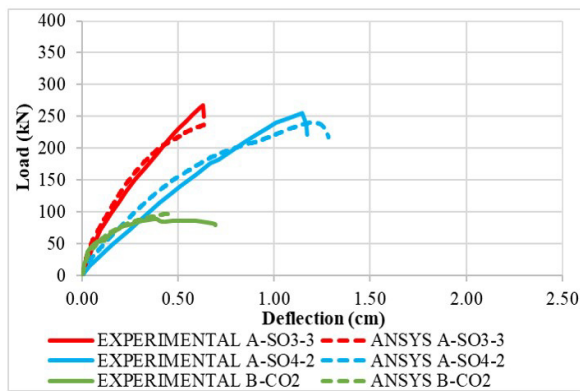
Figure 21. Load vs. midspan deflection diagram for beams with debonding failure.
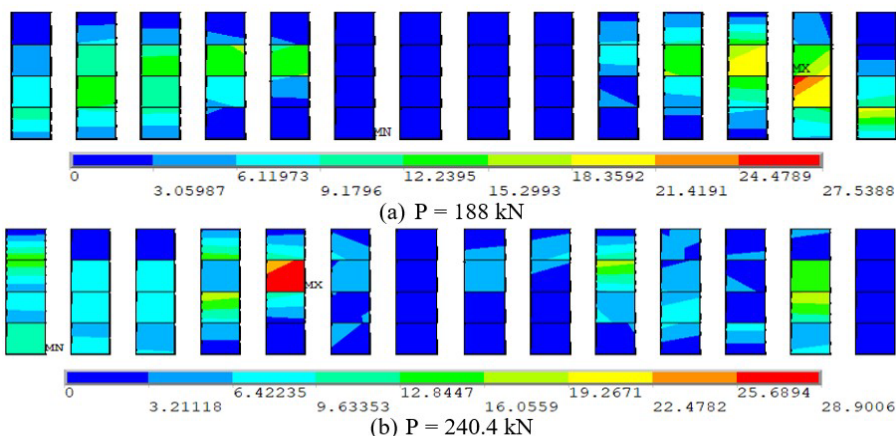

(a) P = 188 kN

(b) P = 240.4 kN

Figure 22. Evolution of the principal stress σ_1 in the CFRP strengthening for beam A-SO3-3 (kN/cm^2).

Figures 23-24 show that the concrete-strengthening interface reached the maximum bond stress (0.366 kN/cm^2) and the maximum slip (0.0169 cm), respectively. This indicates that the debonding of the CFRP strengthening occurred in the shear span, reproducing the behavior observed in the experimental test carried out by Khalifa [19]. Beam A-SO4-2 presented a similar behavior. Figure 25 shows the stress distribution in the reinforcement, and Figures 26-27 show the bond stress and slip at the interface, respectively. It was observed in Figure 28, for beam B-CO2, that the regions of maximum stress are located in the shear span and that this stress value is much lower than the ultimate stress of CFRP (350 kN/cm^2). It was also verified, in Figures 29-30, that the beam reached the maximum bond stress (0.324 kN/cm^2) for a load of approximately 85 kN and the maximum slip (0.0180 cm) for a load of 96 kN, respectively. This indicates that strengthening debonding occurs in the numerical simulation, as observed in the experimental test. Figure 31 illustrates the failure of beams A-SO3-3 and B-CO2.
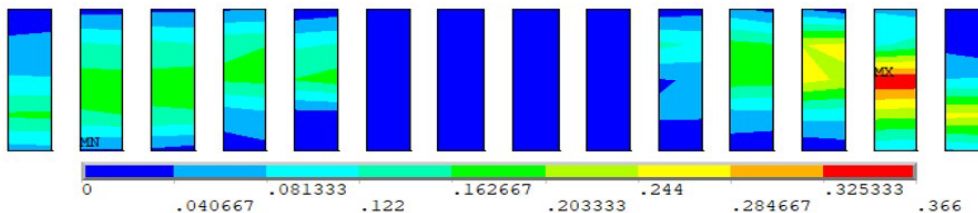

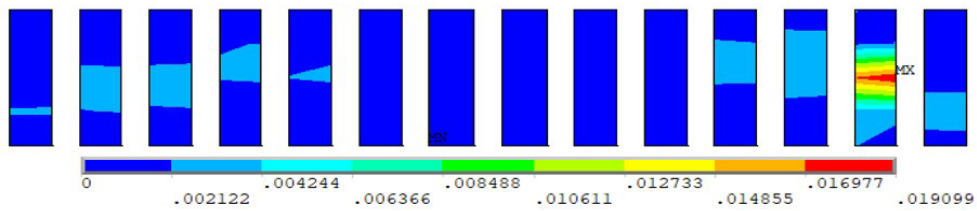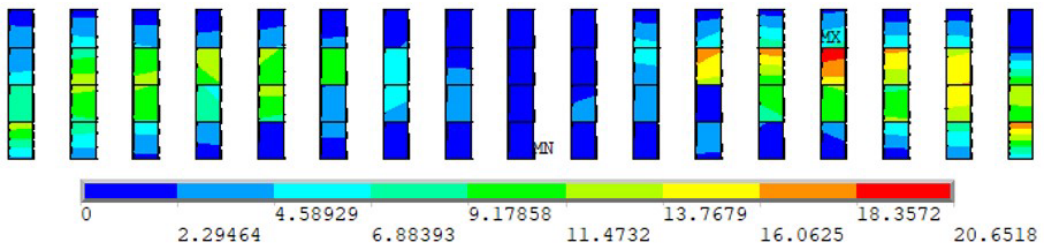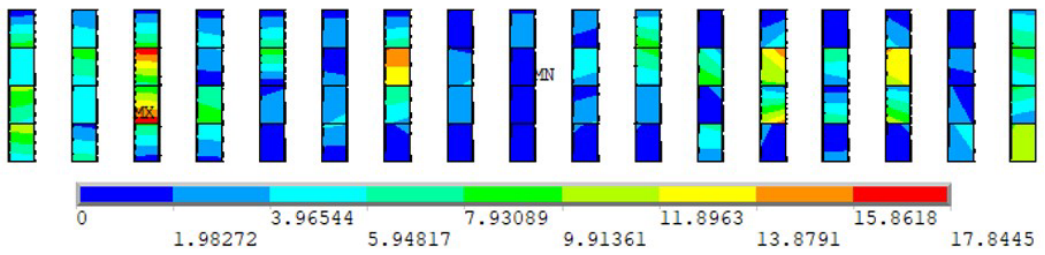**Figure 23.** Bond stress in the interface of beam A-SO3-3 (kN/cm^2).

Rev. IBRACON Estrut. Mater., vol. 16, no. 3, e16304, 2023

14/21

Figure 24. Slip in the interface of beam A-SO3-3 (cm).

(a) P = 150 kN

(b) P = 238.9 kN

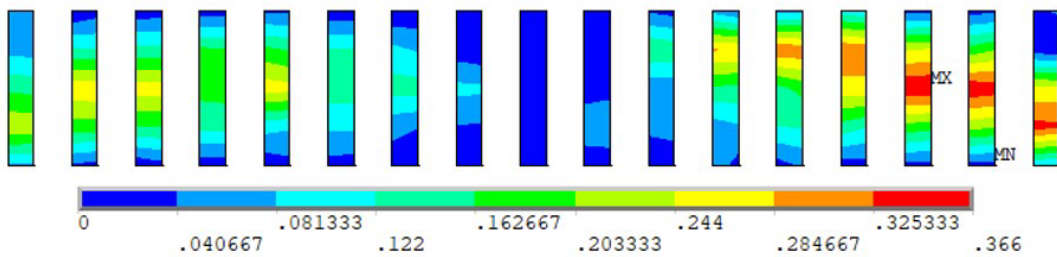**Figure 25.** Evolution of the principal stress σ_1 in the CFRP strengthening for beam A-SO4-2 (kN/cm^2).

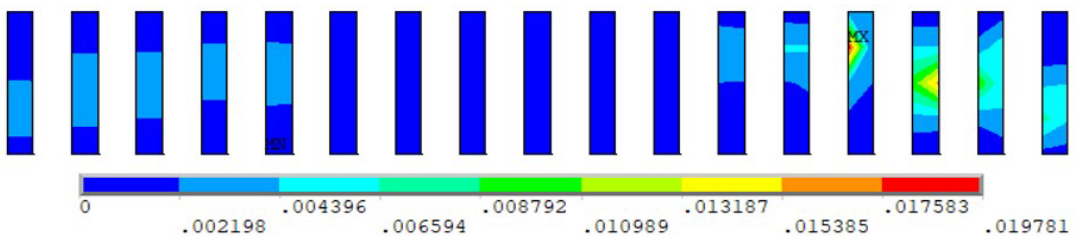**Figure 26.** Bond stress in the interface of the beam A-SO4-2 (kN/cm^2).
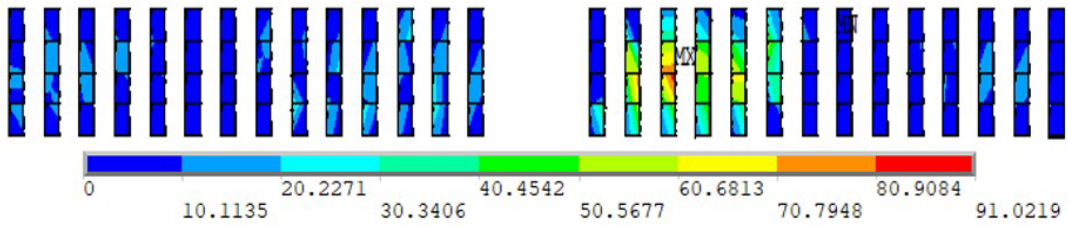

Figure 27. Slip in the interface of beam A-SO4-2 (cm).

Rev. IBRACON Estrut. Mater., vol. 16, no. 3, e16304, 2023

15/21

Figure 28. Principal stress σ_1 in the CFRP strengthening of beam B-CO2 (kN/cm^2).
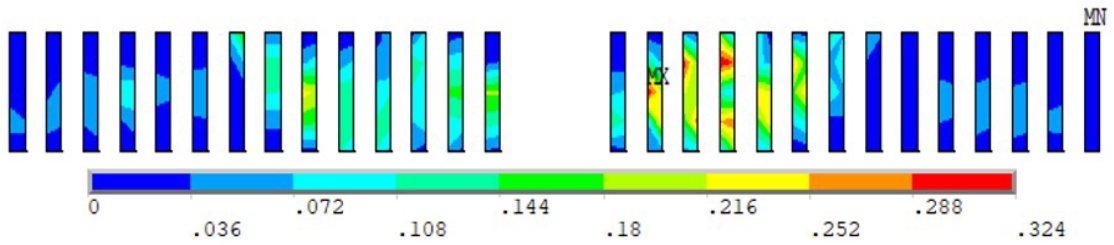

Figure 29. Bond stress in the interface of beam B-CO2 (kN/cm^2).
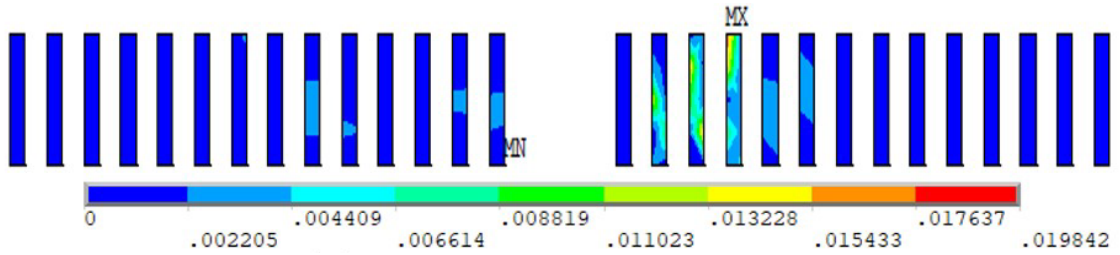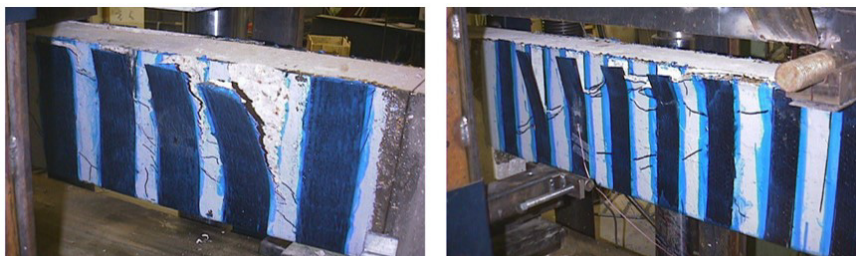

Figure 30. Slip in the interface of beam B-CO2 (cm).

(a) A-SO3-3   (b) B-CO2

Figure 31. Failure modes observed in the experiments [19].

6.4 Flexural failure

Figure 32 presents the comparison between the experimental and numerical results obtained from the proposed modeling, in terms of load vs. midspan deflection for beams B-CF2 and B-CF4.
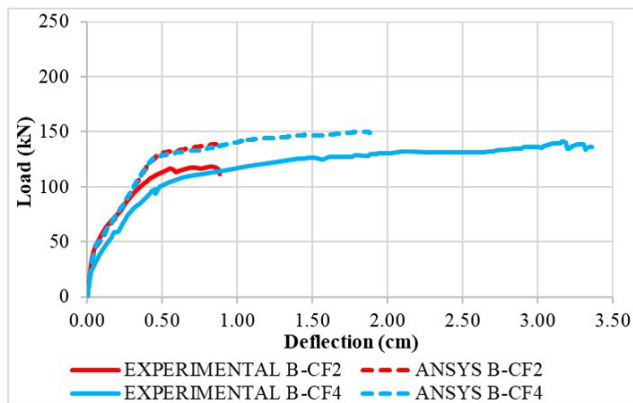
Figure 32. Load vs. midspan deflection diagram for beams with bending failure.

According to the computational model, the longitudinal reinforcement yields at the ultimate condition, as shown in Figures 33-34 for beams B-CF2 and B-CF4, respectively. This indicates that failure occurs due to bending. Figure 35 shows the stress distribution in the CFRP strengthening of beam B-CF2. The bottom strengthening, Figure 35b, presents more significant stresses than those at the lateral strengthening, Figure 35a, due to the bending failure mode of the structural element.

When evaluating the bond stresses and slips at the concrete-strengthening interface, it can be observed that, at the rupture of beam B-CF2, the interface presents the maximum value of bond stress (0.479 kN/cm^2), Figure 36, as well as of slip (0.0148 cm), Figure 37, indicating that the strengthening had a debonding failure. The debonding of the strengthening, after the failure of the beam due to bending, was also observed in the experimental test. It was observed for beam B-CF4 that the CFRP strengthening at the bottom face reached its ultimate stress value (350 kN/cm^2), Figure 38c, which corroborates that the bending failure caused the strengthening to fail, which is in agreement with what was observed in the experimental test. Figure 39 illustrates the failure of beams B-CF2 and B- CF4.
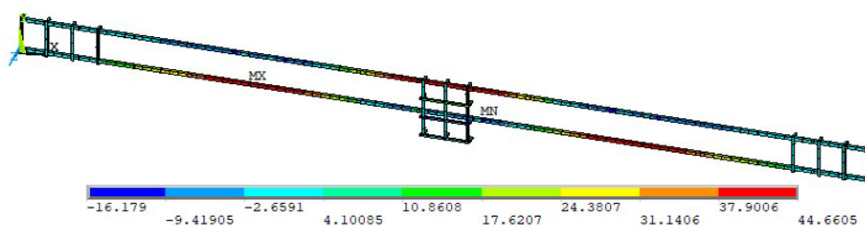

Figure 33. Stress σ_x in the reinforcement of beam B-CF2 (kN/cm^2).
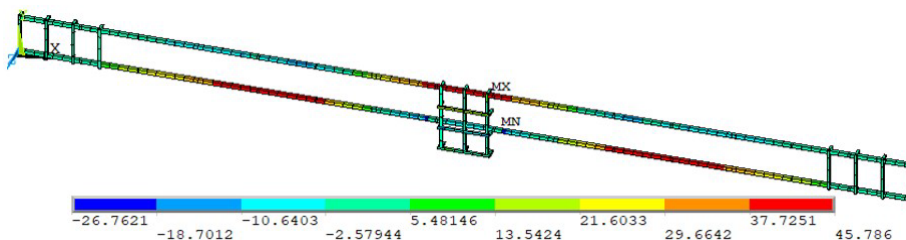
Figure 34. Stress σ_x in the reinforcement of beam B-CF4 (kN/cm^2).

Rev. IBRACON Estrut. Mater., vol. 16, no. 3, e16304, 2023

17/21

(a) Lateral strengthening

(b) Bottom strengthening
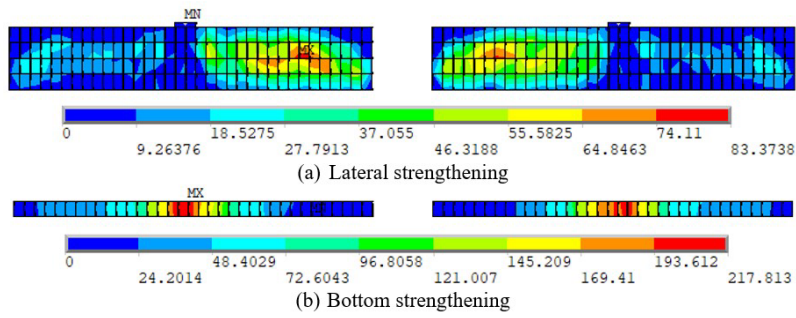
Figure 35. Principal stress σ_1 in the CFRP strengthening of beam B-CF2 (kN/cm^2).
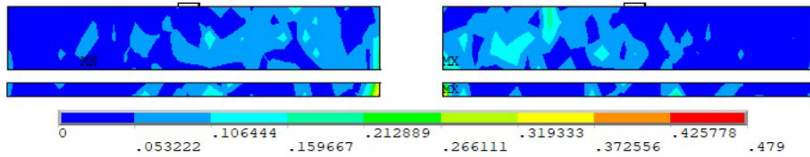
Figure 36. Bond stress in the interface of beam B-CF2 (kN/cm^2).
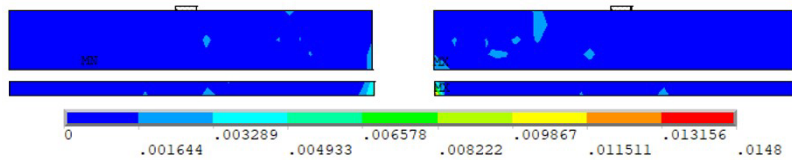
Figure 37. Interface slip of beam B-CF2 (cm).

(a) Top strengthening

(b) Lateral strengthening

(c) Bottom strengthening
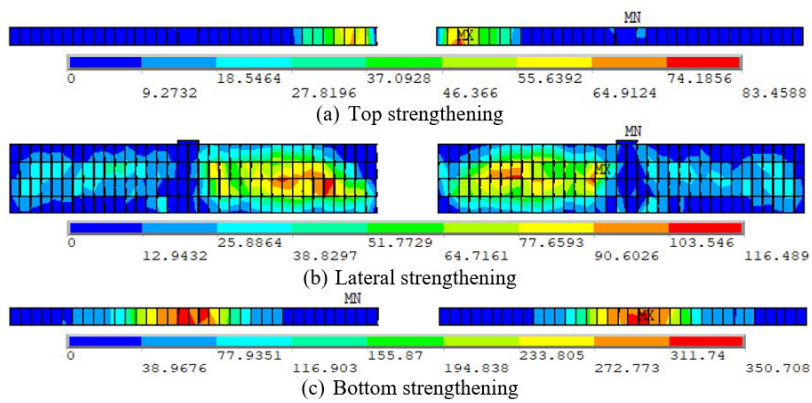
Figure 38. Principal stress σ_1 in the CFRP strengthening of beam B-CF4 (kN/cm^2).

(a) B-CF2   (b) B-CF4
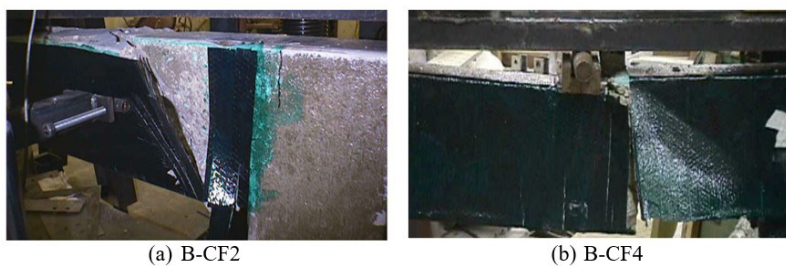
Figure 39. Failure modes observed in the experiments [19].

Rev. IBRACON Estrut. Mater., vol. 16, no. 3, e16304, 2023

18/21

6.5 Summary of Results

Table 4 presents the type of reinforcement for each beam, the experimental and numerical results of failure mode and ultimate load, and the variation of that load for the twenty-one beams. The numerical simulations identified the same failure mode observed in the experimental tests for all the beams in Series A. In addition, ultimate load values were close to those observed by Khalifa [19]. Nine beams presented a variation in the ultimate load of up to 10%, and three beams had a slightly higher variation, with a maximum value of 16.6%.

For the beams in group B, the numerical simulations identified the same failure mode observed in the experimental tests for eight of the nine beams. The only beam that did not show the same experimental failure mode was beam B-CO3. In this case, it was found that, at the ultimate condition, the maximum bond stress and slip values were lower than the values established for this group of beams, thus indicating that the numerical analysis was interrupted when the concrete failed. Probably the reinforcement debonding observed in the experimental test was a post-rupture effect, which was not identified in the numerical simulation.

Regarding the ultimate load values, two beams had the same ultimate load observed in the experimental tests, five beams had a variation of less than 15%, and two beams had variations greater than 15%. Therefore, it was found that, in general, the proposed model could accurately predict the beams' behavior in terms of failure mode and ultimate load.

Table 4. Summary of test results.

Nº	Specimen designation	CFRP shear reinforcement	Experimental		Numerical		Variation (%)
			Failure mode	Load (kN)	Failure mode	Load (kN)	
1	A-SW3-1	-	Shear	252.8	Shear	249.9	-1.1
2	A-SW3-2	Two plies (90°/0°)	Splitting	354.6	Splitting	355.3	0.2
3	A-SW4-1	-	Shear	201.2	Shear	231.6	15.1
4	A-SW4-2	Two plies (90°/0°)	Splitting	361.6	Splitting	372.8	3.1
5	A-SO3-1	-	Shear	151	Shear	151	0
6	A-SO3-2	U-wrap strips, 50 @ 125mm	Debonding	261.9	Debonding	235	-10.3
7	A-SO3-3	U-wrap strips, 75 @ 125mm	Debonding	267.1	Debonding	240.4	-10.0
8	A-SO3-4	One-ply continuous U-wrap	Debonding	289	Debonding	337.1	16.6
9	A-SO3-5	Two plies (90°/0°)	Splitting	339.4	Splitting	321.2	-5.4
10	A-SO4-1	-	Shear	129.4	Shear	126.3	-2.4
11	A-SO4-2	U-wrap strips, 50 @ 125mm	Debonding	254.9	Debonding	240.5	-5.6
12	A-SO4-3	One-ply continuous U-wrap	Splitting	311.1	Splitting	341.5	9.8
13	B-CW1	-	Shear	175	Shear	175	0
14	B-CW2	Two plies (90°/0°)	Splitting	214	Splitting	241	12.6
15	B-CO1	-	Shear	48	Shear	43	-10.4
16	B-CO2	U-wrap strips, 50 @ 125mm	Debonding	88	Debonding	99	12.5
17	B-CO3	One-ply continuous U-wrap	Debonding	113	Splitting	140	23.9
18	B-CF1	-	Shear	93	Shear	93	0
19	B-CF2	One-ply continuous U-wrap	Flexural	119	Flexural	139	16.8
20	B-CF3	Two plies (90°/0°)	Flexural	131	Flexural	150	14.5
21	B-CF4	One-ply; totally wrapped	Flexural	140	Flexural	150	7.1

7 CONCLUSIONS

This work aimed to present a FEM computational program to simulate the behavior of reinforced concrete beams shear-strengthened with CFRP laminates through the customization of the software ANSYS, version 19.2. The results showed that the non-linear models considered could accurately predict the behavior of the tested beams selected from the literature, both in terms of load vs. deflection, as well as when ultimate loads and failure modes were evaluated.

In addition, the ANSYS post-processing visual resources allowed the analysis of stress and strain distributions in the concrete, in the steel rebars and stirrups, and in the CFRP strengthening system considered, as well as facilitating the evaluation of the bond stresses and slips at the concrete-strengthening interface.

It was observed that the simply supported beams A-SW3-1, A-SW4-1, A-SO3-1, and A-SO4-1, and the continuous beams B-CW1, B -CO1, and B-CF1, failed by shear. This confirmed what was already expected in the experiments since they had no strengthening and were indeed designed to fail in shear. Nevertheless, the simply supported beams, A-SW3-2, A-SW4-2, A-SO3-5, and A-SO4-3, and the continuous beam, B-CW2, which were strengthened with CFRP, did not reach the maximum bond stress and slip values at the interface. There was no strengthening debonding, and the concrete failed by reaching stresses and strains above its limits, agreeing again with the experiments, which showed concrete splitting.

Three different behaviors were observed in the numerical simulations for the beams with experimental failure mode due to CFRP debonding. The first one was observed in the simply supported beams strengthened with CFRP strips (A-SO3-2, A-SO3-3, and A-SO4-2), where the interface reached the maximum bond stress followed by a maximum slip in the shear length (between a support and the concentrated load). There was a reduction in the beam stiffness exactly at the CFRP debonding. Then, the stresses decreased toward one end of the beam, reaching the maximum value in the strips located on the opposite end when the ultimate load approached. The second behavior was observed in the simply supported beam with continuous strengthening, A-SO3-4, and in the continuous beam with strip strengthening, B-CO2. The failure of these beams occurred when CFRP debonding took place, with the interfaces reaching the maximum slip value at the ultimate load. The third behavior occurred for the continuous beam with continuous strengthening, B-CO3, wherein the maximum bond stress and slip values were lower than the limiting values that would lead to a collapse. In this case, the numerical analysis was interrupted when the concrete failed. Therefore, the strengthening debonding observed in the experiments was probably a post-rupture effect.

Lastly, one more failure mode observed was due to bending and occurred in the tests of the continuous beams B-CF2, B-CF3, and B-CF4, which had their structural response satisfactorily simulated numerically.

ACKNOWLEDGEMENTS

REFERENCES

[1] S. J. E. Dias, "Investigação experimental e analítica no reforço ao corte de vigas de betão armado com a técnica da inserção de laminados de CFRP," Ph.D. dissertation, Esc. Eng., Univ. Minho, Guimarães, Portugal, 2008.

[2] H. H. Mhanna, R. A. Hawileh, and J. A. Abdalla, "Shear behavior of RC T-beams externally strengthened with anchored high modulus carbon fiber-reinforced polymer (CFRP) laminates," *Compos. Struct.*, vol. 272, p. 114198, May 2021, http://dx.doi.org/10.1016/j.compstruct.2021.114198.

[3] P. B. Soares, "Simulação através do Método dos Elementos Finitos do reforço ao esforço cortante de vigas de concreto utilizando polímeros reforçados com fibras de carbono," Master thesis, Prog. Pós-Grad. Eng. Civil, Univ. Fed. Rio Grande do Sul, Porto Alegre, Brazil, 2022.

[4] B. M. Lazzari, A. Campos Fo., P. M. Lazzari, and A. R. Pacheco, "Using element-embedded rebar model in ANSYS for the study of reinforced and prestressed concrete structures," *Comput. Concr.*, vol. 19, pp. 347–356, Apr. 2017, http://dx.doi.org/10.12989/cac.2017.19.4.347.

[5] P. M. Lazzari, A. Campos Fo., B. M. Lazzari, A. R. Pacheco, and R. Gomes, "Numerical simulation of the constructive steps of a cable-stayed bridge using ANSYS," *Struct. Eng. Mech.*, vol. 69, pp. 269–281, Feb. 2019, http://dx.doi.org/10.12989/sem.2019.69.3.269.

[6] I. S. Hoffman, B. M. Lazzari, A. Campos Fo., P. M. Lazzari, and A. R. Pacheco, "Finite element numerical simulation of a cable-stayed bridge construction through the progressive cantilever method," *Struct. Concr.*, vol. 23, pp. 632–651, Feb. 2022, http://dx.doi.org/10.1002/suco.202100662.

[7] N. S. Ottosen, "A failure criterion for concrete," *J. Eng. Mech. Div.*, vol. 103, no. 4, pp. 527–535, 1977.

[8] Fédération Internationale du Betón, *fib Model Code for Concrete Structures 2010*. Lausanne, Switzerland: FIB, 2013.

[9] E. Hinton, *Numerical Methods and Software for Dynamic Analysis of Plates and Shells*. Swansea, UK: Pineridge Press Limited, 1988.

[10] E. P. Titello, "Análise da confiabilidade de vigas em concreto armado reforçado com fibras de aço em relação aos esforços transversais," Master thesis, Prog. Pós-Grad. Eng. Civil, Univ. Fed. Rio Grande do Sul, Porto Alegre, Brazil, 2020.

[11] P. M. Lazzari, A. Campos Fo., B. M. Lazzari, and A. R. Pacheco, "Structural analysis of a prestressed segmented girder using contact elements in ANSYS," *Comput. Concr.*, vol. 20, pp. 319–327, Sep. 2017, http://dx.doi.org/10.12989/cac.2017.20.3.319.

[12] G. G. Machado, A. Campos Fo., P. M. Lazzari, B. M. Lazzari, and A. R. Pacheco, "Numerical simulation by the finite element method of the constructive steps of a precast prestressed segmental bridge," *Struct. Eng. Mech.*, vol. 85, no. 2, pp. 163–177, Jan. 2023, http://dx.doi.org/10.12989/sem.2023.85.2.163.

[13] F. D. M. Sarturi, "Simulação computacional de estruturas de concreto reforçadas com aço e compósitos de fibra de carbono," Master thesis, Prog. Pós-Grad. Métod. Num. Eng., Univ. Fed. Paraná, Curitiba, Brazil, 2014.

[14] Z. Ouyang and G. Li, "Cohesive zone model based analytical solutions for adhesively bonded pipe joints under torsional loading," *Int. J. Solids Struct.*, vol. 46, no. 5, pp. 1205–1217, Mar. 2009, http://dx.doi.org/10.1016/j.ijsolstr.2008.10.021.

[15] M. V. Medeiros, "Simulação numérica do comportamento de peças fletidas reforçadas com PRFC," Master thesis, Prog. Pós-Grad. Eng. Civil, Univ. Fed. Rio Grande do Sul, Porto Alegre, Brazil, 2019.

[16] ANSYS, Inc., *ANSYS Help System Version 19.2*. Canonsburg, PA, USA: ANSYS, Inc., 2021.

[17] Fédération Internationale du Betón, *Externally Bonded FRP Reinforcement for RC Structures: Bulletin D'information, N. 14*. Lausanne, Switzerland: FIB, 2001.

[18] X. Z. Lu, J. G. Teng, L. P. Ye, and J. J. Jiang, "Bond–slip models for FRP sheets/plates bonded to concrete," *Eng. Struct.*, vol. 27, no. 6, pp. 920–937, May 2005, http://dx.doi.org/10.1016/j.engstruct.2005.01.014.

[19] A. Khalifa, "Shear performance of reinforced concrete beams strengthened with advanced composites," Ph.D. dissertation, Struct. Eng. Depart., Alexandria Univ., Alexandria, Egypt, 1999.

[20] A. Khalifa and A. Nanni, "Rehabilitation of rectangular simply supported RC beams with shear deficiencies using CFRP composites," *Constr. Build. Mater.*, vol. 16, no. 3, pp. 135–146, Jan. 2002.

[21] A. Khalifa, A. Belarbi, and A. Nanni, "Shear performance of RC members strengthened with externally bonded FRP wraps," in *Proc. 12th World Conf. Earthq. Eng.*, New Zealand National Society for Earthquake Engineering , Org. (Auckland, New Zealand), Jan. 2000, pp. 1–8.

[22] A. Khalifa, G. Tumialan, A. Nanni, and A. Belarbi, "Shear strengthening of continuous RC beams using externally bonded CFRP sheets," in *Proc. 4th Int. Symp. FRP Reinf. Concr. Struct.*, American Concrete Institute, Org. (Baltimore, MD, USA), Nov. 1999, pp. 995–1008.

Rev. IBRACON Estrut. Mater., vol. 16, no. 3, e16304, 2023

21/21